

Multimodality in the search for new physics in pulsar timing data and the case of kination-amplified gravitational-wave background from inflation

BOHUA LI ¹, JOEL MEYERS ², AND PAUL R. SHAPIRO ³

¹*Guangxi Key Laboratory for Relativistic Astrophysics, School of Physical Science and Technology, Guangxi University Nanning, 530004, People's Republic of China*

²*Department of Physics, Southern Methodist University, Dallas, TX 75275, USA*

³*Department of Astronomy, The University of Texas at Austin, Austin, TX 78712, USA*

ABSTRACT

We investigate the kination-amplified inflationary gravitational-wave background (GWB) interpretation of the signal recently reported by various pulsar timing array (PTA) experiments. Kination is a post-inflationary phase in the expansion history dominated by the kinetic energy of some scalar field, characterized by a stiff equation of state $w = 1$. Within the inflationary GWB model, we identify two modes which can fit the current data sets (NANOGrav and EPTA) with equal likelihood: the kination-amplification (KA) mode and the ordinary, non-kination-amplification (no-KA) mode. The multimodality of the likelihood motivates a Bayesian analysis with nested sampling. We analyze the free spectra of current PTA data and mock free spectra constructed with higher signal-to-noise ratios, using nested sampling. The analysis of the mock spectrum designed to be consistent with the best fit to the NANOGrav 15 yr (NG15) data successfully reveals the expected bimodal posterior for the first time while excluding the reheating mode that appears in the fit to the current NG15 data, making a case for our correct treatment of potential multimodal posteriors arising from future PTA data sets. The resultant Bayes factor is $\mathcal{B} \equiv \mathcal{Z}_{\text{no-KA}}/\mathcal{Z}_{\text{KA}} = 2.9 \pm 1.9$, indicating comparable statistical significance between the two modes. Given the theoretical model-building challenges of producing highly blue-tilted primordial tensor spectra, the KA mode has the advantage of requiring a less blue primordial spectrum, compared with the no-KA mode. The synergy between future cosmic microwave background polarization, pulsar timing and laser interferometer measurements of gravitational waves will help resolve the ambiguity implied by the multimodal posterior in PTA-only searches.

1. INTRODUCTION

The field of gravitational-wave (GW) astronomy recently witnessed a major breakthrough brought by various pulsar timing array (PTA) collaborations, NANOGrav (G. Agazie et al. 2023), EPTA & InPTA (EPTA Collaboration et al. 2023), PPTA (D. J. Reardon et al. 2023) and CPTA (H. Xu et al. 2023), who concurrently reported strong evidence for a stochastic gravitational-wave background (SGWB) signal in the nanoHertz frequency band. The signature interpulsar Hellings-Downs (HD) correlation curve (R. W. Hellings & G. S. Downs 1983) has been measured up to 4.6 σ statistical significance.

While the confirmation of this signal is underway, interpretation of the existing data has already drawn tremendous attention among the broader astrophysics and high-energy physics community. Beyond the stan-

dard interpretation that the nanohertz SGWB is sourced by inspiraling supermassive black hole binaries (SMBHBs; M. Rajagopal & R. W. Romani 1995; A. H. Jaffe & D. C. Backer 2003; A. Sesana et al. 2004), new-physics models may provide a better fit to the measured free spectrum (A. Afzal et al. 2023; EPTA Collaboration et al. 2024; G. Sato-Polito et al. 2023). Hence, this potential SGWB signal offers abundant opportunities for early-Universe cosmology (e.g., S. Vagnozzi 2023; D. G. Figueroa et al. 2024; J. Ellis et al. 2024).

Cosmological interpretations of the PTA data can be roughly classified as inflationary or non-inflationary signals. Inflationary SGWBs are expected from tensor vacuum fluctuations of the inflaton (L. P. Grishchuk 1974; A. A. Starobinskiĭ 1979; L. F. Abbott & M. B. Wise 1984) or spectator fields (J. L. Cook & L. Sorbo 2012; R. Namba et al. 2016; R. R. Caldwell & C. Devulder 2018), and their post-inflationary amplification (M. Giovannini 1998, 2008; L. A. Boyle & A. Buonanno 2008; B. Li et al. 2017). Non-inflationary SGWBs are produced by causal physics such as first-order phase transitions (M.

Kamionkowski et al. 1994; M. Hindmarsh et al. 2014; P. Schwaller 2015; C. J. Moore & A. Vecchio 2021; Z. Arzoumanian et al. 2021; X. Xue et al. 2021), topological defects (Y. Cui et al. 2018; P. Auclair et al. 2020; J. Ellis & M. Lewicki 2021; S. Blasi et al. 2021; N. Ramberg & L. Visinelli 2021), preheating (S. Khlebnikov & I. Tkachev 1997; R. Easther et al. 2007; K. Jedamzik et al. 2010), scalar fluctuations (K. N. Ananda et al. 2007; D. Baumann et al. 2007; G. Domènech 2021; Y.-F. Cai et al. 2023; G. Franciolini et al. 2023), etc.

In view of the plenitude of models to be tested by the same PTA data sets, carefully implemented methodology for model selection/comparison is key to drawing robust conclusions about any potential new physics. Current model selection methods are mainly based on the Bayes factor, $\mathcal{B}_{10} \equiv \mathcal{Z}_1/\mathcal{Z}_0$, defined as the ratio of the evidence of two models. However, it is understood that the current PTA data are not informative enough to make the Bayes factors free from the “prior volume effect”, i.e., their exact values depend strongly on the range of priors adopted for the parameters (A. Afzal et al. 2023; EPTA Collaboration et al. 2024). Better measurements of the SGWB spectrum are required, therefore, to minimize the prior volume effect and derive stable Bayes factors for new-physics models.

In this letter, we shall address another subtlety in the analysis and interpretation of PTA data regarding the search for new physics, namely the *multimodal* posterior distribution of model parameters. Such a posterior contains disjoint high-likelihood clusters (modes), while each mode may bear a distinctive physical interpretation. As an example, A. Afzal et al. (2023) performed a Bayesian fit to the NANOGrav 15yr data using the inflationary SGWB model that allows for a primordial blue tilt (positive tensor spectral index n_t), and found a bimodal posterior where the signal can be explained by either the tensor perturbations that reentered the horizon during radiation domination (RD) or those that reentered during reheating. However, this “reheating mode” has a spectral index of $n_t - 2$ in the SGWB spectrum today, which requires a notably large n_t to fit the PTA signal. Its best-fit parameters may thus be in conflict with the linearity of primordial tensor fluctuations, as we show in this paper. Instead, we herein consider another case for a potential multimodal posterior: the inflationary SGWB with kination amplification (S. Kuroyanagi et al. 2011; B. Li et al. 2017; C. Caprini & D. G. Figueroa 2018; D. G. Figueroa & E. H. Tanin 2019; Y. Gouttenoire et al. 2021; R. T. Co et al. 2022). Kination is an early phase in the expansion history in which the Universe is dominated by the kinetic energy of some scalar field (B. Spokoiny 1993; M. Joyce 1997;

R. T. Co et al. 2020), also dubbed a “stiff phase,” since the equation of state (EoS) during kination is that of a relativistically-stiff perfect fluid, i.e. $w \equiv \bar{P}/\bar{\rho} = 1$ (B. Li et al. 2014). When kination is present, the kination-amplified (also referred to as “stiff-amplified”) part of the inflationary SGWB spectrum today has index $n_t + 1$, instead of the primordial index n_t , which introduces a new mode that can fit the same PTA data within the inflationary SGWB model (B. Li & P. R. Shapiro 2021).

In contrast to the prior volume effect, multimodality in the posterior becomes more substantial as data get more informative. Therefore, it is crucial to take into account the possibility of multimodality in the analysis of future PTA data. In addition to the common model selection exercise, “mode selection” within one model needs to be performed when possible. To this end, nested sampling (J. Skilling 2006) provides a robust method to explore multimodal posteriors. We here apply the nested sampler implemented by the PolyChord package (W. J. Handley et al. 2015a,b) and evaluate the Bayes factor between the two modes of the inflationary SGWB (with kination amplification or without).

The purpose of this paper is to demonstrate the necessity of considering multimodality (and hence nested samplers) when interpreting the current and future PTA data sets, by the case study of the kination-amplified inflationary SGWB model, a noteworthy model per se. The rest of the paper is organized as follows. We describe our model in Section 2 and the data used in this paper in Section 3. Our results on the bimodal posteriors are shown in Section 4 and relevant discussions are presented in Section 5. We conclude in Section 6.

2. MODEL: KINATION-AMPLIFIED SGWB

The description of the kination-amplified inflationary SGWB follows closely B. Li & P. R. Shapiro (2021). Tensor metric perturbations produced by inflation are assumed to satisfy a power-law initial power spectrum, $\Delta_t^2(f) = A_t (f/f_{\text{CMB}})^{n_t}$, where the tensor amplitude A_t is related to the scalar amplitude by the tensor-to-scalar ratio, $r \equiv A_t/A_s$, and $k_{\text{CMB}} \equiv 2\pi f_{\text{CMB}}/c = 0.05 \text{ Mpc}^{-1}$ is the cosmic microwave background (CMB) pivot scale (Planck Collaboration et al. 2020a). Canonical single-field slow-roll inflation generates a slightly red-tilted primordial tensor spectrum that satisfies the consistency relation, $n_t = -r/8$. However, various nonstandard scenarios can predict a significant blue tilt (L. A. Boyle et al. 2004; A. Stewart & R. Brandenberger 2008; P. Creminelli et al. 2014; Y.-F. Cai et al. 2015; T. Fujita et al. 2019; M. Baumgart et al. 2022). In this work, we relax the consistency relation and treat n_t as an independent parameter.

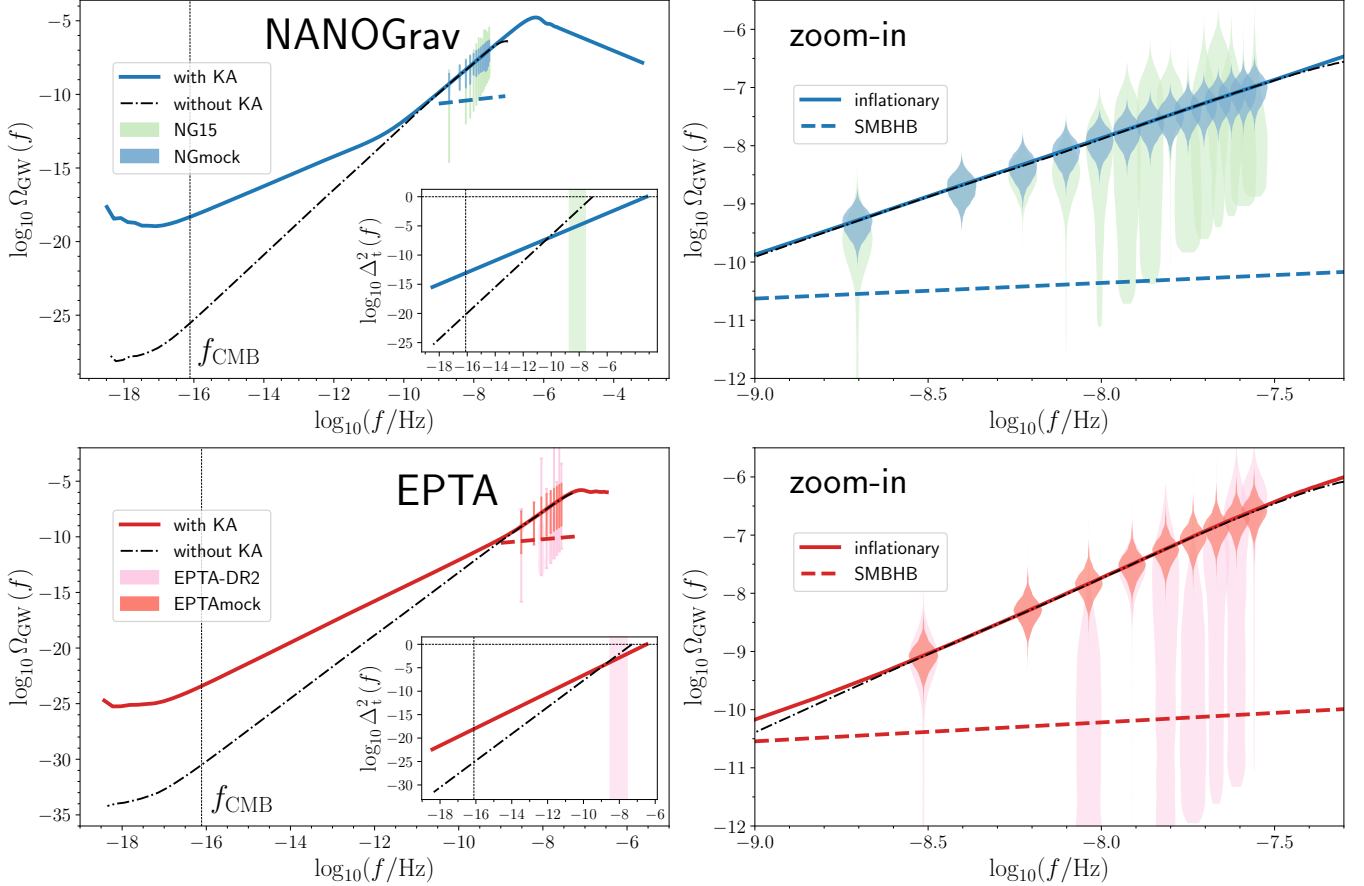


Figure 1. Inflationary SGWB spectra with or without kination amplification. The free spectra obtained from the current PTA data sets as well as our mock free spectra are indicated by the shaded violins: the NG15 and NGmock spectra in the upper panels, the EPTA-DR2 and EPTAmock spectra in the lower panels. The right panels zoom in on the free spectra. In all panels, the inflationary SGWB spectrum curves illustrate the best fits to the corresponding *mock spectra*, colored solid curves for the kination-amplification (KA) mode and black dash-dotted curves for the no-KA mode. The colored dashed lines indicate the accompanying SMBHB component in the KA mode. The insets in the left panels show the blue-tilted primordial tensor spectra, where the nonlinearity cutoffs are illustrated (cf. Appendix A). The vertical shaded regions denote the PTA band.

After reentering the horizon, inflationary tensor perturbations form a SGWB. Its energy spectrum today is given by

$$\Omega_{\text{GW}}(f) \equiv \frac{d\Omega_{\text{GW}}}{d \ln f} = \Delta_t^2(f) \frac{(2\pi f)^2 T^2(f)}{12H_0^2}, \quad (1)$$

where $T(f) \equiv h(f)/h_{\text{ini}}(f)$ is the tensor transfer function, $h(f)$ is the Fourier-space tensor perturbation today and $h_{\text{ini}}(f)$ is its initial superhorizon value. In general, the tensor transfer function is nontrivial and its accurate theoretical prediction must be calculated numerically. We solve the exact tensor wave equation for each frequency iteratively to take account of the backreaction of the SGWB energy density on the expansion history (cf. Appendix A). Our numerical scheme is described in B. Li & P. R. Shapiro (2021) and now available as the `stiffGwpy` package (link provided at the end of the paper). On the other hand, the tensor transfer function

follows a simple power law for wavelengths that reentered the horizon during an era of a *constant* EoS, so that the GW spectrum in the corresponding frequency range can be expressed as

$$\Omega_{\text{GW}}(f) \propto \Delta_t^2(f) \left(\frac{f a_f}{H_0} \right)^2 \propto f^{n_t + \frac{2(3w_f - 1)}{1 + 3w_f}}, \quad (2)$$

where a_f is the scale factor at which the tensor perturbation of frequency f reentered the horizon, $2\pi f \equiv a_f H(a_f)$, and w_f is the EoS parameter then (L. A. Boyle & P. J. Steinhardt 2008; B. Li et al. 2017). Therefore, on top of the primordial tensor spectral index, kination/stiff amplification introduces an additional blue tilt for frequencies with $w_f = 1$, so that $\Omega_{\text{GW}}(f) \propto f^{n_t + 1}$ in this frequency range, as shown by Eq. (2).

We consider a simple extension to the base Λ CDM model, in which the thermal history of the Universe starts in kination and then transitions into RD prior

to Big Bang nucleosynthesis (BBN), $w_{\text{RD}} = 1/3$. Kination is modeled by a stiff fluid ($w_s = 1$) and the kination-to-radiation transition is parameterized by $\kappa_{10} \equiv (\rho_s/\rho_\gamma)|_{T=10 \text{ MeV}}$, the ratio of the stiff-fluid density to the photon density at 10 MeV (S. Dutta & R. J. Scherrer 2010). We assume that the inflationary phase ends into a prolonged reheating epoch dominated by the coherent oscillations of the inflaton field, so $w_{\text{re}} = 0$. The end of reheating marks the onset of kination. In this work, we fix all base- Λ CDM parameters to their *Planck-2018* best-fit values, so our model contains the following free parameters only: $\{r, n_t, \kappa_{10}, T_{\text{re}}, \Delta N_{\text{re}}\}$, where T_{re} is the temperature at the end of reheating and ΔN_{re} is the number of e -folds during reheating. The primordial tensor spectrum in this model is given by the power law described above *only* for $f < f_{\text{cut}}$, where f_{cut} is a UV cutoff on the primordial power spectrum which excludes the pathological nonlinear regime at high frequencies; see the insets in the left panels of Fig. 1. Note that this new UV cutoff is necessary for a consistent description of a blue-tilted primordial spectrum, but has unfortunately been neglected in some previous studies. Further details of the model are elaborated in Appendix A.

Altogether, our model results in a *broken-power-law* energy spectrum for the kination-amplified inflationary SGWB today, $\Omega_{\text{GW}}(f)$ (B. Li & P. R. Shapiro 2021; M. Benetti et al. 2022), as illustrated in Fig. 1. Wavelengths that reentered during RD, kination and reheating have spectral indices of n_t , $n_t + 1$ and $n_t - 2$, respectively. If $\kappa_{10} \gtrsim 10^{-2}$, the kination phase is important for the PTA frequency band. If $\kappa_{10} \ll 10^{-2}$, the frequency corresponding to the kination-to-radiation transition exceeds the PTA band, so that our inflationary SGWB model effectively reduces to the ordinary, non-kination-amplified mode in the PTA band.

3. DATA ANALYSIS

The presence of an SGWB induces an HD-correlated, common-spectrum (red-noise) process to the timing residuals/delays measured by PTAs. The GW spectrum today is thus related to the timing-residual power spectral density (e.g., C. J. Moore & A. Vecchio 2021; G. Agazie et al. 2023), such that

$$\Omega_{\text{GW}}(f) = \frac{2\pi^2 f^2}{3H_0^2} h_c^2(f) = \frac{8\pi^4 f^5}{H_0^2} T_{\text{obs}} \Phi(f), \quad (3)$$

where $h_c(f)$ is the characteristic strain of the SGWB, T_{obs} is the timing baseline and $\Phi(f)$ is the variance of the Fourier components of timing residuals.

In this letter, we analyze the free spectra obtained from the NANOGrav 15yr (NG15, The NANOGrav Collaboration 2023) and the EPTA DR2new (EPTA-DR2, J. Antoniadis et al. 2023) data sets, illustrated by

the light-shaded violins in Fig. 1. For each free spectrum, we perform a Bayesian search for the kination-amplified inflationary SGWB in the presence of a GW foreground from SMBHBs. We do not multiply the NG15 and EPTA-DR2 likelihoods in our analysis but rather consider them separately, since the two data sets contain overlapping pulsars (G. Agazie et al. 2024). A proper combination of various PTA data sets will be provided by the forthcoming IPTA's third data release.

Beyond current data sets, we consider mock data with improved signal-to-noise ratios (S/Ns) to investigate the sensitivity required for future PTAs to overcome the prior volume effect and detect the kination-amplification mode. We generate two power-law mock free spectra with high S/Ns, labeled NGmock and EPTAmock, each with the mean spectral index and frequency bins of the NG15 and EPTA-DR2 data, respectively. They are illustrated by the uniform-shaped, dark-shaded violins in Fig. 1. While the sensitivity of realistic PTAs typically has a non-uniform frequency dependence, each of our mock spectra assumes a uniform uncertainty across its respective frequency bins, set to the smallest uncertainty of the currently measured free spectrum.⁴ Fig. 1 shows that both the kination-amplification (KA) mode and the non-kination-amplification (no-KA) mode can fit the mock spectra equally well. Therefore, we expect the emergence of bimodality in the corresponding analysis results. Note that here the no-KA mode exclusively refers to the case in which the PTA signal is fit by the wavelengths that reentered the horizon during RD, since the reheating mode of spectral index $n_t - 2$ cannot simultaneously fit the mock spectra and satisfy the linearity threshold, as the insets in the left panels of Fig. 1 imply.

Our Bayesian analyses are performed through nested sampling as well as the traditional Markov Chain Monte Carlo (MCMC) sampling, using the *cobaya* code (J. Torrado & A. Lewis 2019, 2021). We assume uniform prior distributions for the aforementioned parameters concerning the inflationary SGWB and kination: $n_t \in [-1, 6]$, $\log_{10} \kappa_{10} \in [-7, 3]$, $\log_{10}(T_{\text{re}}/\text{GeV}) \in [-3, 7]$, $\Delta N_{\text{re}} \in [0, 40]$. For the tensor-to-scalar ratio, we adopt $\log_{10} r \in [-40, 0]$ or $[-20, 0]$ for the NG15 & NGmock analyses, and $\log_{10} r \in [-25, 0]$ for the EPTA-DR2 & EPTAmock analyses. By contrast, a multivariate Gaussian prior is used for parameters concerning the SGWB from SMBHBs (cf. Appendix A), adopting the same model as in A. Afzal et al. (2023), $h_c(f) = A_{\text{BHB}} (f/f_{\text{yr}})^{(3-\gamma_{\text{BHB}})/2}$.

⁴ In either the NG15 and EPTA-DR2 free spectrum, it is the second lowest frequency bin that currently has the highest S/N (see Fig. 1).

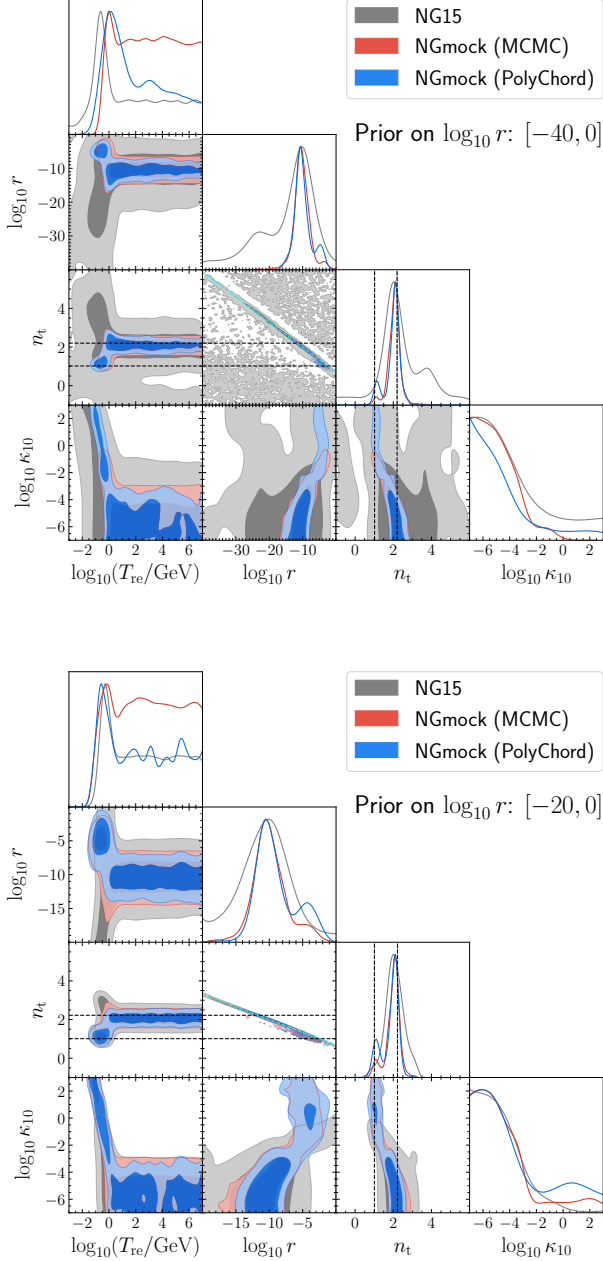


Figure 2. Constraints on the inflationary SGWB model with possible kination amplification from the NG15 and NGmock data. The upper and lower figures show the result obtained using a wide prior on $\log_{10} r$ and that obtained using a narrow prior, respectively. Only a subset of the model parameters is presented, whose posteriors are illustrated by the 68% and 95% 2D contours in the off-diagonal panels and the 1D marginalized distributions in the diagonal panels. The black dashed lines indicate the best-fit values of n_t to the mock spectra, for both the KA and the no-KA modes (cf. Table 1). The cyan dashed lines in the $n_t - \log_{10} r$ panels denote the linear fits to the 2D contours; see Eq. (4).

4. RESULTS: BIMODAL POSTERiors

We now present the results of our Bayesian inference. Fitting the current NG15 and EPTA-DR2 spectra to our model essentially confirms the results in [A. Afzal et al. \(2023\)](#) and [EPTA Collaboration et al. \(2024\)](#), respectively. In these cases, the posterior distributions of the parameters are indicated by the gray contours in Figs. 2 & 3. While some of the 2D posteriors hint at the presence of the KA mode (e.g., the upper left region within the $\log_{10} \kappa_{10} - n_t$ contour with $\kappa_{10} \gtrsim 10^{-2}$ and $n_t \sim 1$), all the 1D marginalized distributions of the model parameters exhibit dominance of the ordinary, no-KA mode. In this regime, the PTA data are basically fit by an inflationary SGWB of spectral index n_t . The strong degeneracy between n_t and r is also recovered; our NG15 analyses result in the following approximate linear relationship:

$$n_t \simeq -0.13 \log_{10} r + 0.7, \quad (4)$$

slightly different from that given by [A. Afzal et al. \(2023\)](#). In addition to the no-KA mode, our NG15 analysis with a wide prior on $\log_{10} r$ yields the secondary reheating mode shown in the upper figure of Fig. 2, similar to what [A. Afzal et al. \(2023\)](#) found.

The reheating mode is nevertheless absent in the posteriors resulted from our Bayesian fits to the high-S/N mock data. Unlike NG15, the NGmock free spectrum has high-S/N data points at the highest frequencies in the PTA band that cannot be fit by the GW spectrum in the reheating mode, since the latter is subject to the UV cutoff at those frequencies, as explained in Section 3. Thus, while the reheating mode appears in the NG15 result (despite the UV cutoff) due to the large uncertainties in the NG15 data at high frequencies, it is however excluded by NGmock. Generally, the reheating mode is likely to be disfavored in the future, as long as a correct UV prescription is implemented.

On the other hand, the analyses of the high-precision NGmock free spectrum reveal the expected KA vs. no-KA bimodality. In fact, our `PolyChord` nested sampling finds two posterior clusters corresponding to the KA and the no-KA modes. As a result, the 2D contours of the posterior distribution reconstructed from the NGmock spectrum in Fig. 2 (blue contours) show two visible peaks in all panels. The 1D marginalized posteriors of n_t and $\log_{10} r$ also exhibit the bimodality. It is important to note that the KA mode is invisible in the NG15 fit *only* because of the prior volume effect: the volume of its best-fit region in the parameter space is significantly smaller than those of the no-KA and the reheating modes. The reason for this is that the poor sensitivity of the current NG15 data can accommodate

larger fractions of the prior volume in those modes due to the wider tails of their distributions. Only when most of those volumes are excluded by the high-S/N mock data can the KA mode emerge. In summary, the NGmock spectrum disfavors the reheating mode but yields a bimodal posterior of the KA and the no-KA modes.

The exclusion of the reheating mode leads to approximately zero likelihood for regions in the parameter space with $\log_{10} r < -20$. Therefore, we opt to report the results of the NGmock analyses obtained using a narrow prior on $\log_{10} r$ for the rest of the paper, shown in the lower figure of Fig. 2. The result obtained by nested sampling has $n_t = 1.29^{+0.13}_{-0.42}$ for the KA mode and $n_t = 2.04^{+0.26}_{-0.19}$ for the no-KA mode (68% credible intervals). This confirms the interpretation that in the KA mode, the PTA data are fit by a kination-amplified inflationary SGWB of spectral index $n_t + 1$. The constraints on all model parameters as well as their best-fit values are presented in Table 1.

Given the bimodal posterior, we can compare the statistical weights of the two modes by means of the Bayes factor, as typically done for model selection. The Bayes factor for the no-KA versus KA mode is defined as the ratio of their evidences, $\mathcal{B} \equiv \mathcal{Z}_{\text{no-KA}}/\mathcal{Z}_{\text{KA}}$, such that a large value ($\mathcal{B} > 10$) would indicate strong evidence in favor of the no-KA mode. By contrast, our PolyChord analysis yields only $\mathcal{B} = 2.9 \pm 1.9$, interpreted as between ‘negligibly small’ and ‘substantial’ according to the Jeffreys scale (H. Jeffreys 1961). Hence, the high-precision NGmock data are statistically compatible with (not against) the KA interpretation. As a matter of fact, even the result of the corresponding MCMC analysis exhibit some degree of bimodality, indicated by the red contours in Fig. 2. However, the MCMC analysis shows quantitative differences from the one obtained by nested sampling. Since nested samplers converge more efficiently for multimodal posteriors and calculate evidences on the fly (W. J. Handley et al. 2015b; L. Lancaster et al. 2017), we opt to report the Bayes factor above from the PolyChord analysis.

In addition to the Bayes factor, it is also useful to compare the maximum posterior ratios of the two modes, $\mathcal{R} \equiv \max(\mathcal{P}_{\text{no-KA}})/\max(\mathcal{P}_{\text{KA}})$, associated with the best-fit models listed in Table 1 (illustrated in Fig. 1). We find that $\mathcal{R} = 0.8$ for NGmock, so the global best fit to the NGmock spectrum is actually given by the KA mode. This is in contrast to the Bayes factor above, which marginally favors the no-KA mode. Yet no contradiction arises, because what the Bayes factor or the evidence ratio compares is the posterior-weighted *volumes* of the two modes. Furthermore, we will see in Section 5 that the Bayes factor defined here depends on

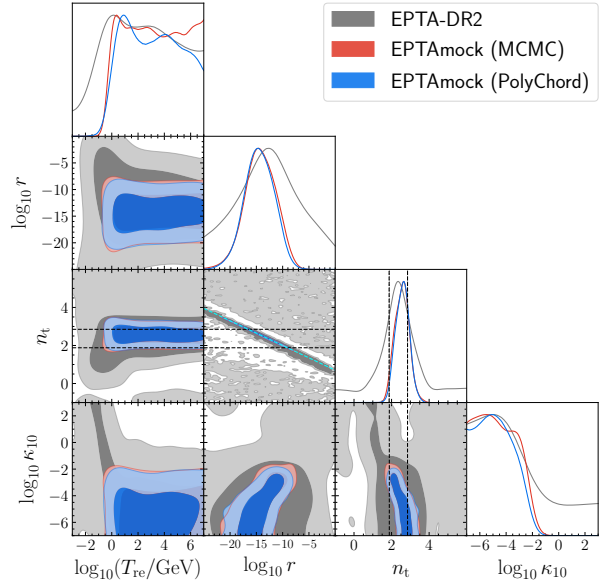


Figure 3. Same as in Fig. 2, but for the EPTA-DR2 and EPTAmock data.

the spectral index of the data. This will explain why the posterior resulting from the EPTAmock spectrum does not appear to be bimodal (see Fig. 3). Even if we cannot compute the Bayes factor in this case, the global best fit to the EPTAmock spectrum is again provided by the KA mode, supporting the existence of bimodality. The maximum posterior ratio for EPTAmock is $\mathcal{R} = 1.0$.

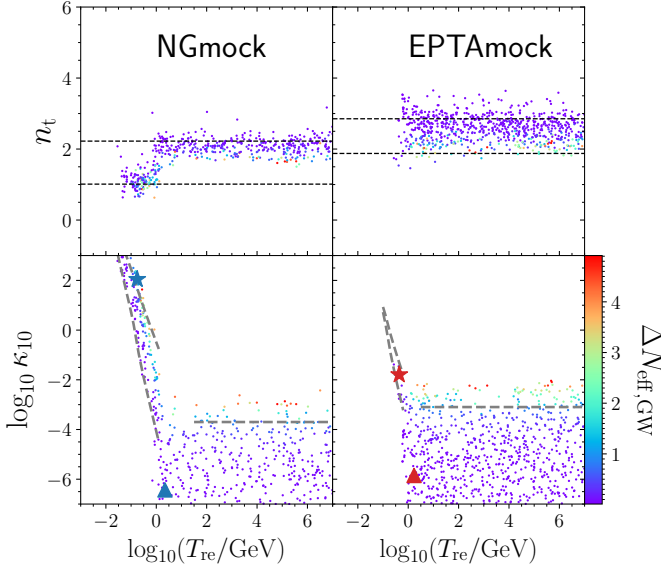
5. DISCUSSION

The above analysis results for the current and mock PTA data imply that the statistical significance of the secondary KA mode (hence the bimodality) is strongly dependent on the sensitivity of the experiment. Existing PTA data cannot decisively exclude low-likelihood regions (tails of the likelihood) in the parameter space. As a result, the prior choice can severely influence the marginalized posteriors, or evidences, for modes that span large prior volumes. For this reason (the prior volume effect), EPTA Collaboration et al. (2024) did not attempt any Bayesian model selection on the origin of the SGWB signal. The same caveat is known to occur in other fields as well, such as the interpretation of the DESI full-shape clustering data (DESI Collaboration et al. 2024), referred to as the ‘‘parameter projection effect’’ there. The DESI team also found that in some cases the mean of the marginalized posterior can be significantly offset from the global best-fit value.

Nevertheless, Bayesian model/mode selection should be less subject to the volume effect as future PTA data become more informative, i.e., low-likelihood regions will no longer boost the evidence of modes with

Table 1. Parameter best fits and 68% credible intervals for the inflationary+SMBHB SGWB model, based on the nested sampling analyses of the mock free spectra.

	NGmock (prior on $\log_{10} r$: $[-20, 0]$)				EPTAmock		
	best-fit values		68% intervals		best-fit values		68% intervals
	KA	no-KA	KA	no-KA	KA	no-KA	
$\log_{10} r$	-4.4	-11.5	$-5.5^{+3.0}_{-1.2}$	$-10.2^{+1.6}_{-1.9}$	-9.4	-16.5	-14.4 ± 2.8
n_t	1.01	2.22	$1.29^{+0.13}_{-0.42}$	$2.04^{+0.26}_{-0.19}$	1.88	2.85	2.58 ± 0.36
$\log_{10} \kappa_{10}$	2.04	-6.43	$-0.5^{+2.6}_{-1.6}$	$-5.05^{+0.93}_{-1.5}$	-1.79	-5.85	< -4.05
$\log_{10}(T_{\text{re}}/\text{GeV})$	-0.76	0.34	$-0.136^{+0.003}_{-0.94}$	$3.3^{+2.5}_{-2.3}$	-0.36	0.23	$3.1^{+1.9}_{-2.9}$
ΔN_{re}	39	23	24^{+20}_{-20}	21 ± 10	13	40	—
$\log_{10} A_{\text{BHB}}$	-15.68	-15.61	$-15.73^{+0.48}_{-0.41}$	$-15.75^{+0.49}_{-0.40}$	-15.60	-15.58	$-15.73^{+0.52}_{-0.41}$
γ_{BHB}	4.73	4.68	4.65 ± 0.33	4.65 ± 0.33	4.67	4.79	4.66 ± 0.35

**Figure 4.** 3D scatter plot with the NGmock sample (left panels) and the EPTAmock sample (right panels). The color bar indicates the value of $\Delta N_{\text{eff,GW}}$ for each point. The stars and the triangles in the lower panels denote the KA and the no-KA best-fits to the mock spectra, respectively. The dashed lines in the upper panels also denote these best fits (same as in the lower figure of Fig. 2), specified in Table 1. The dashed lines in the lower panels indicate the various physical constraints on the KA and the no-KA modes, described by Eqs. (5), (6) and (7).

larger prior volumes significantly. Our analysis of the high-precision NGmock spectrum indeed demonstrates the quenching of the prior volume effect, allowing the bimodality to emerge. The resulting Bayes factor indicates comparable statistical significance between the two modes.

In fact, we are able to identify the physical constraints that shape the high-likelihood regions in the param-

eter space for both modes, which then contribute to the Bayes factor. In the $\log_{10} \kappa_{10} - \log_{10}(T_{\text{re}}/\text{GeV})$ panels of Fig. 4 (lower panels), the KA mode resides in a wedge toward the upper left corner. The boundaries of this wedge have the following physical interpretations:

- The lower bound of the KA subsample is determined by the requirement that the peak frequency of the kination-amplified inflationary SGWB must lie at a value greater than the maximum frequency covered by the PTA band in order for the KA mode to be a good fit. Since the peak frequency in the KA mode corresponds to the frequency of a fluctuation which reentered the horizon at T_{re} (B. Li et al. 2017; B. Li & P. R. Shapiro 2021), the above constraint can be expressed as $f_{\text{re}} > \max(f_{\text{PTA}})$. It yields

$$\log_{10} \kappa_{10} + 4 \log_{10} \frac{T_{\text{re}}}{\text{GeV}} + \frac{4}{3} \log_{10} \frac{g_{*,s}(T_{\text{re}})}{10.75} > -3, \quad (5)$$

where $g_{*,s}(T_{\text{re}})$ is the effective number of relativistic degrees of freedom for entropy at T_{re} . In this work, the thermal history that determines $g_{*,s}(T)$ is adopted from the tabulated function in K. Saikawa & S. Shirai (2020) for $T \geq 10$ MeV and computed using the FortEPiANO package (S. Gariazzo et al. 2019) for $T < 10$ MeV, which incorporates accurate prescriptions for the out-of-equilibrium neutrino decoupling.

- The upper bound of the KA subsample arises from the constraints on the effective number of *extra* relativistic species, $\Delta N_{\text{eff}} \equiv N_{\text{eff}} - N_{\text{eff}}^{\text{SM}}$, where $N_{\text{eff}}^{\text{SM}} = 3.044$ accounts for the standard-model neutrinos (J. J. Bennett et al. 2021). In this case, the kination-amplified inflationary SGWB can contribute a significant ΔN_{eff} (P. D. Lasky et al. 2016; B. Li et al. 2017; B. Li & P. R. Shapiro 2021). While we do not include any

N_{eff} data in the Bayesian analyses here, our model is designed to reject points with $\Delta N_{\text{eff}} > \mathcal{O}(1)$, in accordance with its current observational constraints from BBN and the CMB (R. L. Workman et al. 2022; Planck Collaboration et al. 2020b). The constraint of $\Delta N_{\text{eff,GW}} \lesssim \mathcal{O}(1)$ yields

$$\log_{10} \frac{6}{n_t + 1} + \left(10 + \frac{2}{3} \log_{10} \frac{g_{*,s}(T_{\text{re}})}{10.75}\right) n_t + \log_{10} r + \left(\frac{n_t}{2} + 1\right) \log_{10} \kappa_{10} + 2(n_t + 1) \log_{10} \frac{T_{\text{re}}}{\text{GeV}} \lesssim 6. \quad (6)$$

Eqs. (5) and (6) set the lower and upper limits of the KA wedge, respectively, as illustrated in Fig. 4. Now, let us turn to the no-KA subsample. It is also subject to the constraint of $\Delta N_{\text{eff,GW}} \lesssim \mathcal{O}(1)$. In the no-KA mode, this bound is reached when the inflationary SGWB is actually kination-amplified at frequencies higher than the PTA band. The constraint is therefore on the κ_{10} parameter which determines the transition from kination to the RD era, described by

$$\log_{10} \frac{4}{n_t + 1} + \frac{8.5 - \log_{10} r}{n_t} + \frac{1}{2} \log_{10} \kappa_{10} + \frac{1}{3} \log_{10} \frac{g_{*,s}(T_{\text{kr}})}{10.75} \lesssim 8, \quad T_{\text{kr}} \approx \frac{10 \text{ MeV}}{\sqrt{\kappa_{10}}}, \quad (7)$$

where T_{kr} is the temperature at kination-radiation equality. Eq. (7) is illustrated by the horizontal dashed lines in the lower panels of Fig. 4.

The above physical constraints place hard bounds on the volumes in the parameter space that contribute to the evidences of the modes. They hence impact the relative statistical significance between the no-KA mode and the KA mode, or the Bayes factor. The lower panels of Fig. 4 show that the KA wedge from EPTAmock is much smaller than that from NGmock, explaining why the EPTAmock sample fails to display the KA mode. Furthermore, we can infer from Eqs. (6) and (7) that the volumes of the constrained regions depend on n_t .⁵ In fact, the smaller KA wedge from the EPTAmock spectra results exactly from its higher best-fit value of n_t . Thus, the index of the free spectrum measured by PTAs affects the Bayes factor for the no-KA vs. KA mode comparison, as mentioned in Section 4.

For given PTA data sets, the KA interpretation has the advantage of demanding a less blue-tilted primordial tensor spectrum, compared with the ordinary, no-KA mode (i.e., $n_t + 1$ vs. n_t for the spectral index in Ω_{GW} , the SGWB spectrum today). This is helpful since (i)

plausible early-universe scenarios that predict large blue tensor tilts ($n_t > 1$) and satisfy the N_{eff} constraint at the same time are difficult to realize (W. Giarè et al. 2023), and (ii) the KA interpretation of the PTA signal is less subject to the UV cutoff than the no-KA interpretation (i.e., because it occurs at higher frequencies). Therefore, the kination-amplified inflationary SGWB here does not only present a case study of the multimodality in new-physics searches, but serves as an important model for the origin of the PTA signal on its own.

6. CONCLUSIONS AND OUTLOOK

In this paper, we have investigated the kination-amplified inflationary SGWB interpretation of the recently-reported GW signal from various PTA experiments. Kination refers to a post-inflationary, pre-BBN phase in the expansion history dominated by the kinetic energy of some scalar field, thus characterized by the equation of state $w = 1$. Within the inflationary SGWB model, we have identified two modes which can fit the PTA data sets with equal likelihood: the kination-amplification (KA) mode and the ordinary, no-KA mode. Motivated by the possibility of multimodal posteriors, we have performed Bayesian searches using nested sampling in both the current PTA data and futuristic mock data constructed with higher signal-to-noise ratios. The analysis of the mock free spectrum designed to be consistent with the best fit to the NANOGrav 15 yr data successfully finds the expected bimodal posterior for the first time and, in the meantime, excludes the reheating mode that appears in the fit to the current NG15 data, making a case for our correct treatment of potential multimodal posteriors arising from future PTA data sets. The resultant Bayes factor shows comparable significance between the KA and the no-KA modes. We can conclude from our results that it is critical to take into account correctly any possible multimodality in the new-physics interpretations of PTA data sets. For this purpose, nested-sampling methods should be considered for future PTA analyses, since they can explore multimodal posteriors more efficiently than the traditional MCMC methods.

Finally, we provide a few comments on the implications of future data sets for multimodal posteriors. Although the mock free spectra used in this work are not realistic, they mimic the situation in which the sensitive frequency band of the PTAs widens at the higher end in the future. In the case of the inflationary SGWB with possible kination amplification, more informative PTA data at high frequencies with the same spectral index may further disfavor the no-KA mode. This will happen if the maximum PTA frequency becomes higher

⁵ Since all good fits approximately satisfy the tight relationship between $\log_{10} r$ and n_t in Eq. (4), n_t is effectively the only variable in the constraints (6) and (7).

than the nonlinearity cutoff frequency (detailed in Appendix A) for the no-KA mode, so that the no-KA mode cannot be a good fit. By contrast, the KA mode, with a less blue-tilted primordial spectrum, is less susceptible to the nonlinearity cutoff, as shown in Fig. 1. Therefore, the result of mode selection may shift as future PTA data sets become available.

Moreover, the best-fit spectra of the inflationary SGWB today shown in Fig. 1 encourage the synergy between PTA and other GW data sets. On the high-frequency side, the looser UV cutoff for the KA mode allows for the associated $\Omega_{\text{GW}}(f)$ to extend into the mHz frequency band relevant for the LISA-type, space-borne GW detectors (P. Auclair et al. 2023; W.-H. Ruan et al. 2020; Y. Gong et al. 2021), whereas the single-power-law, no-KA mode may not allow a PTA+LISA joint fit. On the low-frequency side, the less blue-tilted primordial spectrum for the KA mode is also reflected in the shallower lever arm between the CMB scale and the PTA band in $\Omega_{\text{GW}}(f)$ (P. D. Meerburg et al. 2015). Therefore, unlike the no-KA mode, the best-fit value of r for the KA mode could potentially be within reach at the design sensitivity of the next-generation CMB polarization experiments searching for primordial gravitational waves (K. N. Abazajian et al. 2016), allowing

for a CMB+PTA joint fit. In summary, a joint analysis of future CMB polarization, PTA and laser interferometer data will help shed light on models of new physics that may explain observations of the SGWB, and will allow for a quantitative comparison of the various physical mechanisms consistent with the data that give rise to multimodal posteriors from PTA-only searches.

ACKNOWLEDGMENTS

We thank Joseph Romano, Kejia Lee, Siyuan Chen, Zucheng Chen for helpful discussions. BL is supported by the National Natural Science Foundation of China (Grant Nos. 12203012, 12494575) and Guangxi Natural Science Foundation (Grant No. 2023GXNSFBA026114). This work is also supported by the Guangxi Talent Program (“Highland of Innovation Talents”). JM is supported by the US Department of Energy under Grant DE-SC0010129 and by NASA through Grant 80NSSC24K0665. PRS acknowledges support from NASA under Grant No. 80NSSC22K175.

Software: cobaya (J. Torrado & A. Lewis 2019, 2021), PolyChord (W. J. Handley et al. 2015a,b), FortEPiNO (S. Gariazzo et al. 2019), stiffGWpy (<https://github.com/bohuarolandli/stiffGWpy>),

APPENDIX

A. DETAILS OF THE MODEL

Consistent modeling of the blue-tilted inflationary SGWB with possible kination amplification involves the treatment of two more complexities:

- (i) The inflationary SGWB requires a UV cutoff, typically chosen as f_{inf} , corresponding to the horizon scale at the end of inflation. However, when $n_t > 0$, it is possible that the amplitude of the tensor modes in the blue-tilted spectrum reaches unity at some high frequency *below* the f_{inf} cutoff. When this apparent nonlinearity happens, the amplitude must saturate, and one needs a more advanced prescription than linear perturbation theory to treat the UV behavior of the primordial tensor fluctuations (e.g., G. Ye et al. 2024; S. Pi et al. 2024). This pathology is unfortunately overlooked in existing studies which attempt to fit inflationary SGWB models to PTA data, e.g., A. Afzal et al. (2023).

To avoid dealing with the unknown physics beyond the apparent nonlinearity, we keep the single-power-law assumption while imposing another UV cutoff for the primordial tensor spectrum, f_{cut} , at which the tensor power equals unity, $A_t (f_{\text{cut}}/f_{\text{CMB}})^{n_t} \equiv 1$. This cutoff is illustrated in the insets of Fig. 1.

- (ii) As we showed in B. Li & P. R. Shapiro (2021), SGWBs with spectra that are blue-tilted (either because the primordial tensor spectrum is blue-tilted or because kination amplification tilts a flat primordial spectrum blue for wavelengths that entered the horizon after reheating) can make a considerable contribution to the critical density during radiation domination, leading to a nonnegligible backreaction on the expansion history. We account for this backreaction by an iterative numerical scheme developed in B. Li & P. R. Shapiro (2021); see also T. Kite et al. (2022).

As mentioned in Section 2, we solve the exact tensor wave equation for a range of sampled frequencies, using a dynamical system approach. The tensor wave equation is only integrated for the horizon-crossing epoch of each frequency, $2\pi f/aH \in [10^{-3}, e^5]$. After it is well inside the horizon, we switch to the time-averaged solution, as demonstrated in the upper left panel of Fig. 5. The overall numerical solver for the inflationary SGWB with possible kinematic amplification is released as the `stiffGWpy` package. Fig. 5 shows the same example numerical solution as in Fig. 1.

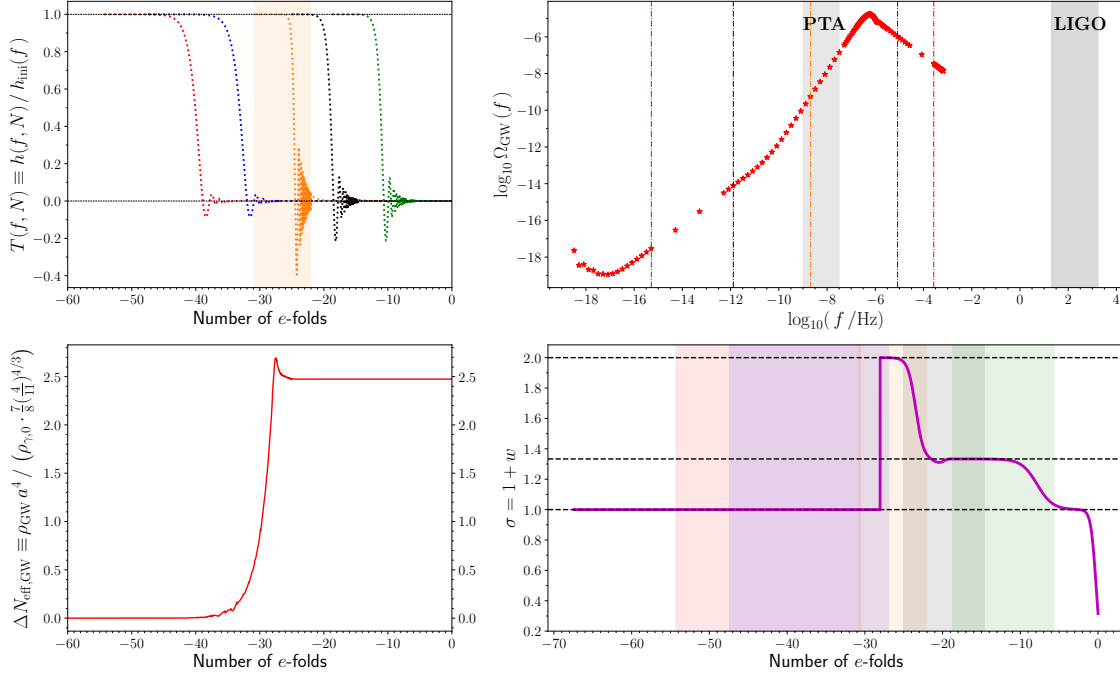


Figure 5. *Upper left:* tensor transfer functions for five example frequencies. The orange vertical shade indicates the horizon-crossing epoch of the corresponding frequency. *Upper right:* Kinematic-amplified inflationary SGWB spectrum today, same as that indicated by the solid curves in the upper panels of Fig. 1. The vertical dash-dotted lines denote the example frequencies illustrated in the upper left panel. *Lower left:* evolution of the effective number of extra relativistic species due to the inflationary SGWB, $\Delta N_{\text{eff,GW}}$. *Lower right:* expansion history described by the evolution of the EoS parameter. The vertical shades indicate the horizon-crossing epochs of the frequencies in the upper left panel.

Apart from the inflationary SGWB, the SGWB from SMBHBs must be taken into account. Following A. Afzal et al. (2023), we adopt a power-law model for the SMBHB component, parameterized by $(\log_{10} A_{\text{BHB}}, \gamma_{\text{BHB}})$. This pair of parameters approximately satisfies a bivariate Gaussian distribution with the following mean and covariance matrix:

$$\mu = (-15.6, 4.7), \quad \sigma = \begin{bmatrix} 0.28 & -0.0026 \\ -0.0026 & 0.12 \end{bmatrix}. \quad (\text{A1})$$

Moreover, the PolyChord nested sampler requires bounded priors, so we impose the following bounded intervals on these parameters: $\log_{10} A_{\text{BHB}} \in [-18, -11]$ and $\gamma_{\text{BHB}} \in [0, 7]$, in addition to the bivariate Gaussian prior.

REFERENCES

- Abazajian, K. N., Adshead, P., Ahmed, Z., et al. 2016, arXiv e-prints, arXiv:1610.02743. <https://arxiv.org/abs/1610.02743>
- Abbott, L. F., & Wise, M. B. 1984, Nuclear Physics B, 244, 541, doi: 10.1016/0550-3213(84)90329-8

- Afzal, A., Agazie, G., Anumarpudi, A., et al. 2023, *ApJL*, 951, L11, doi: [10.3847/2041-8213/acdc91](https://doi.org/10.3847/2041-8213/acdc91)
- Agazie, G., Anumarpudi, A., Archibald, A. M., et al. 2023, *ApJL*, 951, L8, doi: [10.3847/2041-8213/acdac6](https://doi.org/10.3847/2041-8213/acdac6)
- Agazie, G., Antoniadis, J., Anumarpudi, A., et al. 2024, *ApJ*, 966, 105, doi: [10.3847/1538-4357/ad36be](https://doi.org/10.3847/1538-4357/ad36be)
- Ananda, K. N., Clarkson, C., & Wands, D. 2007, *PhRvD*, 75, 123518, doi: [10.1103/PhysRevD.75.123518](https://doi.org/10.1103/PhysRevD.75.123518)
- Antoniadis, J., Arumugam, P., Arumugam, S., et al. 2023,, 2.0 Zenodo, doi: [10.5281/zenodo.8091568](https://doi.org/10.5281/zenodo.8091568)
- Arzoumanian, Z., Baker, P. T., Blumer, H., et al. 2021, *PhRvL*, 127, 251302, doi: [10.1103/PhysRevLett.127.251302](https://doi.org/10.1103/PhysRevLett.127.251302)
- Auclair, P., Blanco-Pillado, J. J., Figueroa, D. G., et al. 2020, *JCAP*, 2020, 034, doi: [10.1088/1475-7516/2020/04/034](https://doi.org/10.1088/1475-7516/2020/04/034)
- Auclair, P., Bacon, D., Baker, T., et al. 2023, *Living Reviews in Relativity*, 26, 5, doi: [10.1007/s41114-023-00045-2](https://doi.org/10.1007/s41114-023-00045-2)
- Baumann, D., Steinhardt, P., Takahashi, K., & Ichiki, K. 2007, *PhRvD*, 76, 084019, doi: [10.1103/PhysRevD.76.084019](https://doi.org/10.1103/PhysRevD.76.084019)
- Baumgart, M., Heckman, J. J., & Thomas, L. 2022, *JCAP*, 2022, 034, doi: [10.1088/1475-7516/2022/07/034](https://doi.org/10.1088/1475-7516/2022/07/034)
- Benetti, M., Graef, L. L., & Vagnozzi, S. 2022, *PhRvD*, 105, 043520, doi: [10.1103/PhysRevD.105.043520](https://doi.org/10.1103/PhysRevD.105.043520)
- Bennett, J. J., Buldgen, G., de Salas, P. F., et al. 2021, *JCAP*, 2021, 073, doi: [10.1088/1475-7516/2021/04/073](https://doi.org/10.1088/1475-7516/2021/04/073)
- Blasi, S., Brdar, V., & Schmitz, K. 2021, *PhRvL*, 126, 041305, doi: [10.1103/PhysRevLett.126.041305](https://doi.org/10.1103/PhysRevLett.126.041305)
- Boyle, L. A., & Buonanno, A. 2008, *PhRvD*, 78, 043531, doi: [10.1103/PhysRevD.78.043531](https://doi.org/10.1103/PhysRevD.78.043531)
- Boyle, L. A., & Steinhardt, P. J. 2008, *PhRvD*, 77, 063504, doi: [10.1103/PhysRevD.77.063504](https://doi.org/10.1103/PhysRevD.77.063504)
- Boyle, L. A., Steinhardt, P. J., & Turok, N. 2004, *PhRvD*, 69, 127302, doi: [10.1103/PhysRevD.69.127302](https://doi.org/10.1103/PhysRevD.69.127302)
- Cai, Y.-F., Gong, J.-O., Pi, S., Saridakis, E. N., & Wu, S.-Y. 2015, *Nuclear Physics B*, 900, 517, doi: [10.1016/j.nuclphysb.2015.09.025](https://doi.org/10.1016/j.nuclphysb.2015.09.025)
- Cai, Y.-F., He, X.-C., Ma, X.-H., Yan, S.-F., & Yuan, G.-W. 2023, *Science Bulletin*, 68, 2929, doi: [10.1016/j.scib.2023.10.027](https://doi.org/10.1016/j.scib.2023.10.027)
- Caldwell, R. R., & Devulder, C. 2018, *PhRvD*, 97, 023532, doi: [10.1103/PhysRevD.97.023532](https://doi.org/10.1103/PhysRevD.97.023532)
- Caprini, C., & Figueroa, D. G. 2018, *Classical and Quantum Gravity*, 35, 163001, doi: [10.1088/1361-6382/aac608](https://doi.org/10.1088/1361-6382/aac608)
- Co, R. T., Dunskey, D., Fernandez, N., et al. 2022, *Journal of High Energy Physics*, 2022, 116, doi: [10.1007/JHEP09\(2022\)116](https://doi.org/10.1007/JHEP09(2022)116)
- Co, R. T., Hall, L. J., & Harigaya, K. 2020, *PhRvL*, 124, 251802, doi: [10.1103/PhysRevLett.124.251802](https://doi.org/10.1103/PhysRevLett.124.251802)
- Cook, J. L., & Sorbo, L. 2012, *PhRvD*, 85, 023534, doi: [10.1103/PhysRevD.85.023534](https://doi.org/10.1103/PhysRevD.85.023534)
- Creminelli, P., Gleyzes, J., Noreña, J., & Vernizzi, F. 2014, *PhRvL*, 113, 231301, doi: [10.1103/PhysRevLett.113.231301](https://doi.org/10.1103/PhysRevLett.113.231301)
- Cui, Y., Lewicki, M., Morrissey, D. E., & Wells, J. D. 2018, *PhRvD*, 97, 123505, doi: [10.1103/PhysRevD.97.123505](https://doi.org/10.1103/PhysRevD.97.123505)
- DESI Collaboration, Adame, A. G., Aguilar, J., et al. 2024, *arXiv e-prints*, arXiv:2411.12022, doi: [10.48550/arXiv.2411.12022](https://doi.org/10.48550/arXiv.2411.12022)
- Domènech, G. 2021, *Universe*, 7, 398, doi: [10.3390/universe7110398](https://doi.org/10.3390/universe7110398)
- Dutta, S., & Scherrer, R. J. 2010, *PhRvD*, 82, 083501, doi: [10.1103/PhysRevD.82.083501](https://doi.org/10.1103/PhysRevD.82.083501)
- Easther, R., Giblin, Jr., J. T., & Lim, E. A. 2007, *PhRvL*, 99, 221301, doi: [10.1103/PhysRevLett.99.221301](https://doi.org/10.1103/PhysRevLett.99.221301)
- Ellis, J., & Lewicki, M. 2021, *PhRvL*, 126, 041304, doi: [10.1103/PhysRevLett.126.041304](https://doi.org/10.1103/PhysRevLett.126.041304)
- Ellis, J., Fairbairn, M., Franciolini, G., et al. 2024, *PhRvD*, 109, 023522, doi: [10.1103/PhysRevD.109.023522](https://doi.org/10.1103/PhysRevD.109.023522)
- EPTA Collaboration, InPTA Collaboration, Antoniadis, J., et al. 2023, *A&A*, 678, A50, doi: [10.1051/0004-6361/202346844](https://doi.org/10.1051/0004-6361/202346844)
- EPTA Collaboration, InPTA Collaboration, Antoniadis, J., et al. 2024, *A&A*, 685, A94, doi: [10.1051/0004-6361/202347433](https://doi.org/10.1051/0004-6361/202347433)
- Figueroa, D. G., Pieroni, M., Ricciardone, A., & Simakachorn, P. 2024, *PhRvL*, 132, 171002, doi: [10.1103/PhysRevLett.132.171002](https://doi.org/10.1103/PhysRevLett.132.171002)
- Figueroa, D. G., & Tanin, E. H. 2019, *JCAP*, 2019, 011, doi: [10.1088/1475-7516/2019/08/011](https://doi.org/10.1088/1475-7516/2019/08/011)
- Franciolini, G., Iovino, A. J., Vaskonen, V., & Veermäe, H. 2023, *PhRvL*, 131, 201401, doi: [10.1103/PhysRevLett.131.201401](https://doi.org/10.1103/PhysRevLett.131.201401)
- Fujita, T., Kuroyanagi, S., Mizuno, S., & Mukohyama, S. 2019, *Physics Letters B*, 789, 215, doi: [10.1016/j.physletb.2018.12.025](https://doi.org/10.1016/j.physletb.2018.12.025)
- Gariazzo, S., de Salas, P. F., & Pastor, S. 2019, *JCAP*, 2019, 014, doi: [10.1088/1475-7516/2019/07/014](https://doi.org/10.1088/1475-7516/2019/07/014)
- Giarè, W., Forconi, M., Di Valentino, E., & Melchiorri, A. 2023, *MNRAS*, 520, 1757, doi: [10.1093/mnras/stad258](https://doi.org/10.1093/mnras/stad258)
- Giovannini, M. 1998, *PhRvD*, 58, 083504, doi: [10.1103/PhysRevD.58.083504](https://doi.org/10.1103/PhysRevD.58.083504)
- Giovannini, M. 2008, *Physics Letters B*, 668, 44, doi: [10.1016/j.physletb.2008.07.107](https://doi.org/10.1016/j.physletb.2008.07.107)
- Gong, Y., Luo, J., & Wang, B. 2021, *Nature Astronomy*, 5, 881, doi: [10.1038/s41550-021-01480-3](https://doi.org/10.1038/s41550-021-01480-3)

- Gouttenoire, Y., Servant, G., & Simakachorn, P. 2021, arXiv e-prints, arXiv:2111.01150, doi: [10.48550/arXiv.2111.01150](https://doi.org/10.48550/arXiv.2111.01150)
- Grishchuk, L. P. 1974, *Zhurnal Eksperimentalnoi i Teoreticheskoi Fiziki*, 67, 825
- Handley, W. J., Hobson, M. P., & Lasenby, A. N. 2015a, *MNRAS*, 450, L61, doi: [10.1093/mnras/slv047](https://doi.org/10.1093/mnras/slv047)
- Handley, W. J., Hobson, M. P., & Lasenby, A. N. 2015b, *MNRAS*, 453, 4384, doi: [10.1093/mnras/stv1911](https://doi.org/10.1093/mnras/stv1911)
- Hellings, R. W., & Downs, G. S. 1983, *ApJL*, 265, L39, doi: [10.1086/183954](https://doi.org/10.1086/183954)
- Hindmarsh, M., Huber, S. J., Rummukainen, K., & Weir, D. J. 2014, *PhRvL*, 112, 041301, doi: [10.1103/PhysRevLett.112.041301](https://doi.org/10.1103/PhysRevLett.112.041301)
- Jaffe, A. H., & Backer, D. C. 2003, *ApJ*, 583, 616, doi: [10.1086/345443](https://doi.org/10.1086/345443)
- Jedamzik, K., Lemoine, M., & Martin, J. 2010, *JCAP*, 2010, 021, doi: [10.1088/1475-7516/2010/04/021](https://doi.org/10.1088/1475-7516/2010/04/021)
- Jeffreys, H. 1961, *Theory of Probability* (Oxford University Press)
- Joyce, M. 1997, *PhRvD*, 55, 1875, doi: [10.1103/PhysRevD.55.1875](https://doi.org/10.1103/PhysRevD.55.1875)
- Kamionkowski, M., Kosowsky, A., & Turner, M. S. 1994, *PhRvD*, 49, 2837, doi: [10.1103/PhysRevD.49.2837](https://doi.org/10.1103/PhysRevD.49.2837)
- Khlebnikov, S., & Tkachev, I. 1997, *PhRvD*, 56, 653, doi: [10.1103/PhysRevD.56.653](https://doi.org/10.1103/PhysRevD.56.653)
- Kite, T., Chluba, J., Ravenni, A., & Patil, S. P. 2022, *MNRAS*, 509, 1366, doi: [10.1093/mnras/stab3125](https://doi.org/10.1093/mnras/stab3125)
- Kuroyanagi, S., Nakayama, K., & Saito, S. 2011, *PhRvD*, 84, 123513, doi: [10.1103/PhysRevD.84.123513](https://doi.org/10.1103/PhysRevD.84.123513)
- Lancaster, L., Cyr-Racine, F.-Y., Knox, L., & Pan, Z. 2017, *JCAP*, 2017, 033, doi: [10.1088/1475-7516/2017/07/033](https://doi.org/10.1088/1475-7516/2017/07/033)
- Lasky, P. D., Mingarelli, C. M. F., Smith, T. L., et al. 2016, *Physical Review X*, 6, 011035, doi: [10.1103/PhysRevX.6.011035](https://doi.org/10.1103/PhysRevX.6.011035)
- Li, B., Rindler-Daller, T., & Shapiro, P. R. 2014, *PhRvD*, 89, 083536, doi: [10.1103/PhysRevD.89.083536](https://doi.org/10.1103/PhysRevD.89.083536)
- Li, B., & Shapiro, P. R. 2021, *JCAP*, 2021, 024, doi: [10.1088/1475-7516/2021/10/024](https://doi.org/10.1088/1475-7516/2021/10/024)
- Li, B., Shapiro, P. R., & Rindler-Daller, T. 2017, *PhRvD*, 96, 063505, doi: [10.1103/PhysRevD.96.063505](https://doi.org/10.1103/PhysRevD.96.063505)
- Meerburg, P. D., Hložek, R., Hadzhiyska, B., & Meyers, J. 2015, *PhRvD*, 91, 103505, doi: [10.1103/PhysRevD.91.103505](https://doi.org/10.1103/PhysRevD.91.103505)
- Moore, C. J., & Vecchio, A. 2021, *Nature Astronomy*, 5, 1268, doi: [10.1038/s41550-021-01489-8](https://doi.org/10.1038/s41550-021-01489-8)
- Namba, R., Peloso, M., Shiraiishi, M., Sorbo, L., & Unal, C. 2016, *JCAP*, 2016, 041, doi: [10.1088/1475-7516/2016/01/041](https://doi.org/10.1088/1475-7516/2016/01/041)
- Pi, S., Sasaki, M., Wang, A., & Wang, J. 2024, *PhRvD*, 110, 103529, doi: [10.1103/PhysRevD.110.103529](https://doi.org/10.1103/PhysRevD.110.103529)
- Planck Collaboration, Akrami, Y., Arroja, F., et al. 2020a, *A&A*, 641, A10, doi: [10.1051/0004-6361/201833887](https://doi.org/10.1051/0004-6361/201833887)
- Planck Collaboration, Aghanim, N., Akrami, Y., et al. 2020b, *A&A*, 641, A6, doi: [10.1051/0004-6361/201833910](https://doi.org/10.1051/0004-6361/201833910)
- Rajagopal, M., & Romani, R. W. 1995, *ApJ*, 446, 543, doi: [10.1086/175813](https://doi.org/10.1086/175813)
- Ramberg, N., & Visinelli, L. 2021, *PhRvD*, 103, 063031, doi: [10.1103/PhysRevD.103.063031](https://doi.org/10.1103/PhysRevD.103.063031)
- Reardon, D. J., Zic, A., Shannon, R. M., et al. 2023, *ApJL*, 951, L6, doi: [10.3847/2041-8213/acdd02](https://doi.org/10.3847/2041-8213/acdd02)
- Ruan, W.-H., Liu, C., Guo, Z.-K., Wu, Y.-L., & Cai, R.-G. 2020, *Nature Astronomy*, 4, 108, doi: [10.1038/s41550-019-1008-4](https://doi.org/10.1038/s41550-019-1008-4)
- Saikawa, K., & Shirai, S. 2020, *JCAP*, 2020, 011, doi: [10.1088/1475-7516/2020/08/011](https://doi.org/10.1088/1475-7516/2020/08/011)
- Sato-Polito, G., Zaldarriaga, M., & Quataert, E. 2023, arXiv e-prints, arXiv:2312.06756, doi: [10.48550/arXiv.2312.06756](https://doi.org/10.48550/arXiv.2312.06756)
- Schwaller, P. 2015, *PhRvL*, 115, 181101, doi: [10.1103/PhysRevLett.115.181101](https://doi.org/10.1103/PhysRevLett.115.181101)
- Sesana, A., Haardt, F., Madau, P., & Volonteri, M. 2004, *ApJ*, 611, 623, doi: [10.1086/422185](https://doi.org/10.1086/422185)
- Skilling, J. 2006, *Bayesian Anal.*, 1, 833, doi: [10.1214/06-BA127](https://doi.org/10.1214/06-BA127)
- Spokoiny, B. 1993, *Physics Letters B*, 315, 40, doi: [10.1016/0370-2693\(93\)90155-B](https://doi.org/10.1016/0370-2693(93)90155-B)
- Starobinskiĭ, A. A. 1979, *Soviet Journal of Experimental and Theoretical Physics Letters*, 30, 682
- Stewart, A., & Brandenberger, R. 2008, *JCAP*, 2008, 012, doi: [10.1088/1475-7516/2008/08/012](https://doi.org/10.1088/1475-7516/2008/08/012)
- The NANOGrav Collaboration. 2023,, v2 Zenodo, doi: [10.5281/zenodo.10344086](https://doi.org/10.5281/zenodo.10344086)
- Torrado, J., & Lewis, A. 2019,, *Astrophysics Source Code Library*, record ascl:1910.019
- Torrado, J., & Lewis, A. 2021, *JCAP*, 2021, 057, doi: [10.1088/1475-7516/2021/05/057](https://doi.org/10.1088/1475-7516/2021/05/057)
- Vagnozzi, S. 2023, *Journal of High Energy Astrophysics*, 39, 81, doi: [10.1016/j.jheap.2023.07.001](https://doi.org/10.1016/j.jheap.2023.07.001)
- Workman, R. L., Burkert, V. D., Crede, V., et al. 2022, *Progress of Theoretical and Experimental Physics*, 2022, 083C01, doi: [10.1093/ptep/ptac097](https://doi.org/10.1093/ptep/ptac097)
- Xu, H., Chen, S., Guo, Y., et al. 2023, *Research in Astronomy and Astrophysics*, 23, 075024, doi: [10.1088/1674-4527/acdfa5](https://doi.org/10.1088/1674-4527/acdfa5)
- Xue, X., Bian, L., Shu, J., et al. 2021, *PhRvL*, 127, 251303, doi: [10.1103/PhysRevLett.127.251303](https://doi.org/10.1103/PhysRevLett.127.251303)
- Ye, G., Zhu, M., & Cai, Y. 2024, *Journal of High Energy Physics*, 2024, 8, doi: [10.1007/JHEP02\(2024\)008](https://doi.org/10.1007/JHEP02(2024)008)